Journal of Materials Chemistry A

Accepted Manuscript

ROYAL SOCIETY OF CHEMISTRY

www.rsc.org/materialsA

Journal of Materials Chemistry A

ARTICLE

Monodisperse and self-assembled Pt-Cu nanoparticles as an efficient electrocatalyst for methanol oxidation reaction

Received 00th January 20xx,
Accepted 00th January 20xx

DOI: 10.1039/x0xx00000x

www.rsc.org/

Xuewei Du[a], Shuiping Luo[a], Hongyu Du[a], Min Tang[a], Xiangdong Huang[b], and Pei Kang Shen*[a]

Monodisperse alloyed PtCu nanoparticles (NPs) have been synthesized via a facile one-pot hydrothermal method. In addition, this is the first time to get self-assembled NPs like a hexagonal array with six-fold symmetry in PtCu NPs system. In our synthesis, oleylamine(OAM) is essential for the appearance of self-assembly of uniform PtCu NPs. These PtCu spheres have a diameter of 4.78±0.28 nm with a Pt-rich skin and are evaluated as the catalyst for methanol oxidation reaction. The activity of the PtCu nanoparticles are 34.81 mA cm^{-2}, while that of the PtCu/C catalysts are 24.6 mA cm^{-2}, which are about 6.216 times and 4.4 times larger than that of the Pt/C catalyst (5.6 mA cm^{-2}). Our studies provide a simple approach to synthesize monodisperse PtCu NPs with Pt-rich skin, making it possible to develop highly active catalyst for methanol oxidation .

Introduction

Direct methanol fuel cells (DMFCs) have attracted considerable attentions among the various green and sustainable technologies on chemical transformations and energy conversion in the past few decades due to their simple design, high energy conversion efficiency, low environmental pollution, convenient fuel transportation, storage and supply[1, 2]. Highly active electrocatalyst is critical for the success of DMFC technology since it can dramatically reduce the over-potential associated with the slow kinetics of anodic methanol oxidation and/or cathodic oxygen reduction[3]. Up to now, platinum (Pt) nanoparticles are catalytically active for the anodic (methanol oxidation reaction, MOR) reaction of the DMFCs[4, 5]. But the high cost of the noble metal platinum and low activities of the anode catalysts at room temperature are still the important issues that hinder the commercialization of DMFCs[6]. Moreover, the electro-oxidation of methanol is intrinsically slow because the intermediate product, carbon monoxide, is known to adsorb strongly onto the pure Pt sites of the catalysts, thereby inhibiting their catalytic functions[7]. In order to solve these problems, bimetallic Pt alloys containing low cost transition metals (such as Cu, Ni, Fe, Pd, etc.) have alternatively been studied[8, 9].

In comparison with the pure Pt nanoparticles, Pt alloys with well-defined morphologies possessing not only large surface areas but also unique structural properties reduce the loading amount of Pt[10, 11] and less precious transition metal can provide oxygenated species at lower potentials for the oxidative removal of the adsorbed COads to prevent the catalysts from deactivating[12], hence enhancing catalytic activities. In particularly, for many kinds of non-noble metals, Cu is one of the earth-abundant elements and can be received easily[13]. In addition, Pt-Cu catalysts are prominent catalysts with a reduced sensitivity toward COads-like intermediates[14, 15]. In the current achievements, Pt-Cu catalysts were successfully synthesized through multi-steps[16, 17], seed-mediated approach[18] or galvanic displacement reaction[19]. These preparation processes are so cumbersome that is not suitable for practical applications. A simple synthesized route was needed. Meanwhile, the synthesis of well-controlled Pt nanocrystals under 10 nm in size remains highly challenge[20, 21], especially with self-assembly and monodispersed properties.

Herein, we describe the preparation of highly monodispersed PtCu nanoparticles with an average size of 4.78 nm through a facile one-pot hydrothermal method. Moreover, we firstly realized the monolayer self-assembly of face-centered cubic (fcc) monodispersed PtCu catalyst with high performance used in direct methanol fuel cells. In this route, N,N-dimethylformamide (DMF) as both solvent and reducing agent, while cetyltrimethyl ammoniumbromide (CTAB) is used as surfactant. In our experiment, part of PtCu nanoparticles were coated on commercial carbon powders and their electrocatalytic properties for methanol electrooxidation were investigated by cyclic voltammetry (CV) and CO-stripping voltammetry. It is observed that all the as-synthesized PtCu and PtCu/C catalysts exhibited higher activity, better stability and CO resistance for methanol oxidation than commercial Pt/C catalysts.

[a] A State Key Laboratory of Optoelectronic Materials and Technologies, School of Physics and Engineering, Sun Yat-sen University, Guangzhou, 510275, P. R. China. E-mail: stsspk@mail.sysu.edu.cn
[b] Automotive Engineering Institute, Guangzhou Automobile Group Co., Ltd, Guangzhou, 510640, PR China

Electronic Supplementary Information (ESI) available: [details of any supplementary information available should be included here]. See DOI: 10.1039/x0xx00000x

Experimental

Materials

For the synthetic process of monodispersed and self-assembly PtCu nanoparticles, we used one-pot hydrothermal method. In details, 10 mL of N,N-dimethylformamide (DMF) were added into fairly clean inner cup of hydrothermal synthesis reactor at first. Then, 350mg of hexadecyltrimethyl ammonium bromide (CTAB) and 62.24mg of $Cu(NO_3)_2 \cdot 3H_2O$ were added into the reaction vessel, respectively. Afterwards, 0.31mL of H_2PtCl_6 (concentration: 32.8 mg/mL) solution was transformed into the reactor. When H_2PtCl_6 solution was injected, the mixture changed from dilute mixture to colloidal condition. After finishing these, the reaction vessel was taken into the outer pot of hydrothermal synthesis reactor and tighten up in order to form a high pressure environment for good reaction. Immediately following, the hydrothermal synthesis reactor was put in the thermostatic oil bath in the 170℃ temperature and keep for 24 hours.

After reaction was stopped and the temperature was cooled down to the room temperature, the product was taken out and added ethanol into it till at the position of 30mL, and the final black catalyst was collected by centrifugation at 4000 rpm for 10 minutes. The process was repeated for three times. Finally, the catalyst was dispersed in 10mL n-hexane for further characterization.

Samples coated on carbon

10mg commercial carbon powders were put in 10mL n-hexane, and then dispersed using ultrasound cleaner to get homogeneous solution. After this, the solution of carbon and catalyst all in 10mL n-hexane were mixed together and on ultrasonic dispersion for one hour. Afterwards, the mixture was stirred for 48 hours. When stirring ends, the solution was centrifuged at 4000 rpm for 10 minutes. The obtained sediment was added into 30mL methanol, and followed by centrifugation, which were repeated for three times. At last, the precipitate was decentralized in absolute ethyl alcohol and conducted for suction filtration. The final product was then dried at 80 ℃ in vacuum.

Self-assembly methods

After reaction was stopped, the product was added ethanol into it till at the position of 30mL, and the final black catalyst was collected by centrifugation at 4000 rpm for 10 minutes. Unlike the above washing way, the obtained precipitate processed ultrasound with 30 mL of ethanol along with 0.5mL of oleylamine (OAM) to be homogeneous suspension, and was then centrifuged at 4000 rpm for 10 minutes. Next, the deposits went on ultrasound only with 30mL of ethanol, and then centrifugation at 4000 rpm for 10 minutes for three times. Finally, the catalyst was dispersed in 10mL n-hexane for further characterization.

Characterizations

Transmission electron microscope (TEM) images were performed on JEOL JEM-2010HR electron microscopy operating at 200 kV. High resolution TEM images of individual nanoparticles were recorded on a FEI Tecnai™ G2 F30 electron microscope at an accelerating voltage of 300 kV. For selected area electron diffraction (SAED) patterns and the TEM measurements, a drop of the nanoparticle solution was dispensed onto a 3-mm carbon-coated nickel (Ni) grid. Powder X-ray diffraction (PXRD) spectra were recorded using a Rigaku D-MAX 200 VPC X-ray diffractometer with Cu Ka radiation (l ~ 1.5405 Å). X-Ray photoemission spectroscopy (XPS) was operated on a Thermo-VG Scientific ESCALAB 250 photoelectron spectrometer equipped with a monochromatic two anode X-ray gun. For the PXRD and XPS measurements, the sample was taken from the catalyst coated on carbon.

Electrochemical measurements

Electrochemical measurements were operated in a standard three-electrode cell with the catalyst-modified glassy carbon electrode (5 mm in diameter) as working electrode connected to a PINE Computer-Controlled Bipotentiostat. A saturated calomel electrode (SCE) electrode was used as the reference electrode. The counter electrode was carbon rod. For the loading of the bimetallic PtCu alloy nanoparticles on commercial carbon powders, the working electrode was a thin layer of nafion-impregnated catalyst cast on a vitreous carbon disk. This electrode catalyst suspension was prepared by ultrasonically dispersing 3.6mg of the PtCu/C into 2mL solution containing 1.8mL of ethanol and 0.2mL of Nafion solution (DuPont, USA). A 10μL of the ink was dispensed onto the 5 mm of glassy carbon disk electrode and the electrode was then dried in room temperature. The catalytic performance of PtCu nanoparticles in room temperature for methanol oxidation reaction (MOR) was measured by cyclic voltammetry. The working electrodes were first activated with cyclic voltammograms (CVs) (−0.2 to 1.0 V at 100mV/s) in N_2-purged 0.5 M H_2SO_4 solution until a steady CV was obtained. To measure methanol electrooxidation, the solution of 0.5M H_2SO_4 + 1M CH_3OH was purged with N_2 gas before measurement, and the CVs were recorded in a potential window between −0.2 and 1.0 V at a scan rate of 50 mV/s in acidic solution. The ECSA of Pt was measured by integrating the charges associated with hydrogen adsorption between −0.2 and 0.1 V and calibrated by the adsorption (210 μC/cm2 Pt) of a monolayer of hydrogen on a polycrystalline Pt surface. For the anodic stripping of CO, CO was used to saturate the H_2SO_4 (0.5 M) electrolyte for 30 min, while the working electrode was held at -0.14 V. The passage of CO was then stopped, and the electrolyte was thoroughly purged with high-purity nitrogen. Next, the adsorbed CO was oxidized by CV with a scan rate of 50mV/s, and the CO stripping curve was taken. Two subsequent CV cycles were also recorded to verify the complete oxidation of the adsorbed CO. Electrochemical durability tests were employed to evaluate the long term performance of the catalysts. Using the same system for a CV test, scanning 1,000 cycles were conducted in the current study with CV curves between −0.2 and 1.0 V in 0.5 M H_2SO_4 + 1 M CH_3OH solution at a scan rate of 100 mV/s.

Results and discussion

The PtCu nanoparticles were synthesized in DMF that had a uniform spheres morphology and size (4.78 ± 0.28 nm). As is known to all, DMF has been widely used as a weak reducing agent with the production of CO at its boiling point (153 °C). The endogenous CO could serve as both a reducing agent and an effective protecting agent during the formation of NPs[22, 23].

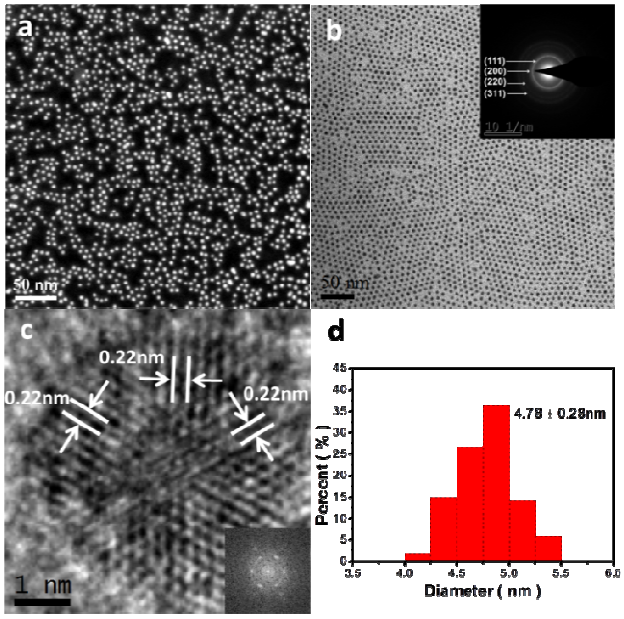

Fig. 1. (a) HAADF-STEM image, (b) TEM image of PtCu nanoparticles, and the inset in b is the SAED pattern, (c)HR-TEM image of single PtCu nanoparticle and the inset in c is the FFT pattern , (d) the size distribution histogram of PuCu nanoparticles.

As seen in Fig.1a, the image shows high-angle-annular-dark-field scanning transmission electron microscopy (HAADF-STEM) pattern of the representative PtCu nanoparticles dropped on the nickel grid without OAM during washing. It is observed that these catalysts exhibit a spherical shape, and are uniformly dispersed without agglomeration, showing its super-duper dispersity. In addition, Fig.S1 further shows the monodispersed property of PtCu nanoparticles. As displayed in Fig.1b, the transmission electron microscope (TEM) micrographs further prove the good dispersity of PtCu alloy nanoparticles. As the comparison, the $Pt_{68}Cu_{32}$ NPs and $Pt_{38}Cu_{62}$ NPs were synthesized by adjusting the ratio of Pt and Cu when starting the experiments. Fig. S2. Shows the TEM images of the $Pt_{68}Cu_{32}$ NPs(a) and $Pt_{38}Cu_{62}$ NPs(b). Although $Pt_{68}Cu_{32}$ NPs dispersed without agglomeration, the particle size was not uniform. For $Pt_{38}Cu_{62}$ NPs, they have uniform size, but were agglomerated. The negative-image selected area electron diffraction (SAED) pattern shown in inset of Figure 1b exhibits several bright continuous concentric rings attributable to the diffusions from the (111), (200) and (311) planes of PtCu nanoparticles referring to alloyed PtCu (PDF# 48-1549), which proves the existence and ratio (1:1) of Pt to Cu elements. To further figure out the detailed structure of the obtained nanospheres, HRTEM image of a single PtCu nanosphere was carefully collected (Fig.1c). An interplanar distance of 0.22nm was clearly revealed, which is consistent with the lattice spacing of the (111) plane in PDF# 48-1549, whose is 0.2191nm. The lattice fringes with spacing of 0.22 nm in the other directions were also found, representing different directions of (111) plane and indicating that most nanoparticles are twinned[23, 24]. The structural feature may result in unique properties where surface atomic structures are critically important[25]. Fast Fourier Transformation (FFT) image shown in illustration of Fig.1c confirms their twinned structures. An accurate data of size statistical analysis was obtained and the size distribution histogram of PtCu nanoparticles was made (Fig.1d). It was found that the typical diameter is between 4 to 5.5 nm with a narrow size distribution, and the average diameter is 4.78 nm ± 0.28nm, which fully exhibits the uniformity of the monodispersed nanospheres.

One of the characteristics of monodispersed nanoparticles is the ability to form ordered close-packed arrays. Herein, for the first time we demonstrate that by washing the product with ethanol containing 1.6 % oleylamine to purify the PtCu nanoparticles, the very uniform PtCu nanoparticles were gradually self-assembled under the function of oleylamine. TEM images (Fig.2a) show all the PtCu NPs can be self-assembled and arranged orderly and regularly. Meanwhile, Fig.2b further clearly shows the self-assembled structure which is similar to a hexagon of graphene structure made up of six particles. Importantly, previous studies showed that oleylamine can serve as an effective ligand in the synthesis of monodisperse Pt or Pt-based nanoparticles[11, 20, 21, 26-28]. In our synthesis, OAM acting as surfactant can provide effective capping ligands having long chains coating on the particles, which along with van der Waals attraction between the particles are the key driving force determining the formation of self-assembly of the monodispersed PtCu NPs[29]. Also, solvent evaporation, attractive depletion forces, Coulomb forces and so on can also be the origin of nanoparticles organizations. Finally, the delicate balance of attractive and repulsive forces results in the formation of nanoparticle self-assembly[30, 31]. Meanwhile, uniform nanocrystals are known to be self-assembled under appropriate conditions[32, 33]. In addition, the nanocrystals self-assembly are highly uniform in both size and shape, while the irregular shaped nanocrystals are excluded from the self-assembly[21]. Therefore, uniform

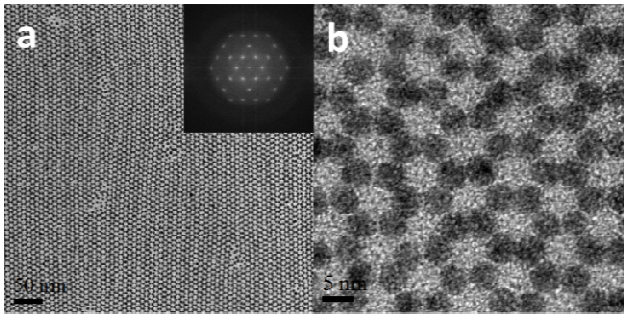

Fig. 2.TEM images of monolayer self-assembled pattern of PtCu nanoparticles: (a) 50nm size (b) 5nm size and the insert in a is the FFT patterns from the corresponding

diameter and good dispersion are another key factor for the self-assembly of PtCu nanoparticles. The narrow size (shown in Fig.1d) of the monodisperse PtCu nanoparticles fully exhibits the uniformity of the nanospheres and further explains the reason of the formation of self-assembly of PtCu nanoparticles. From Fig.S3, we observed that nanoparticles were self-assembled even though in the edge of the sample, which well expounds the integrity of self-assembly. The fast Fourier transform (FFT) pattern from the corresponding TEM images of Fig.2b with 6-fold symmetry agrees with the results in the Fig.2c and 2d, further confirming the self-assembly feature of the PtCu nanoparticles.

The PtCu NPs were coated on commercial carbon powder to be tested for the powder X-ray diffraction (PXRD) and X-ray photoelectron spectroscopy (XPS). TEM images (Fig.S4) of PtCu/C show that PtCu NPs can be coated on carbon powder very uniformly. PXRD (Fig.3a) patterns of the as-synthesized PtCu/C catalysts could be indexed to (111), (200), (220), and (311) diffractions of a face-centered-cubic (fcc) structure with the 2θ peak positions at 41.16°, 47.88°, 70.05° and 84.64° between pure Pt and Cu diffractions[18, 24], respectively, indicating the alloy nature of the reaction product. All these results were judged by the PDF card 48-1549 in XRD database. The Pt/Cu composition is around 1:1, as confirmed by both inductively coupled plasma atomic emission spectroscopy (ICP-AES) and transmission electron microscopy-EDX (TEM-EDX) (Fig. 3b). It is worth noting that as the typical bulk sample, its diffractions from (111) plane which is centered at 2θ around 41.16° is the strongest and further suggest these PtCu NPs are

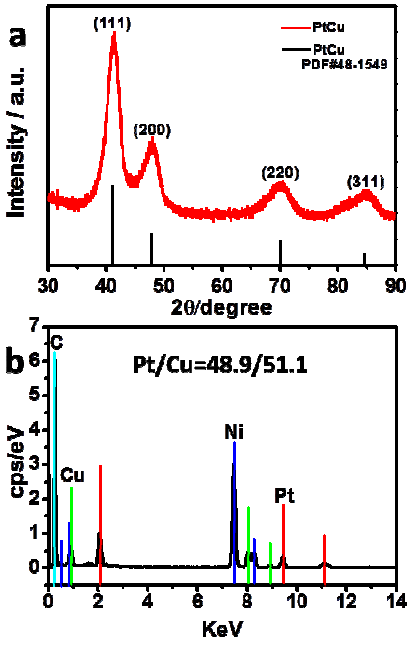

Fig. 3. (a) XRD pattern of PtCu/C catalyst and (b) TEM-EDX spectrum of PtCu nanoparticles.

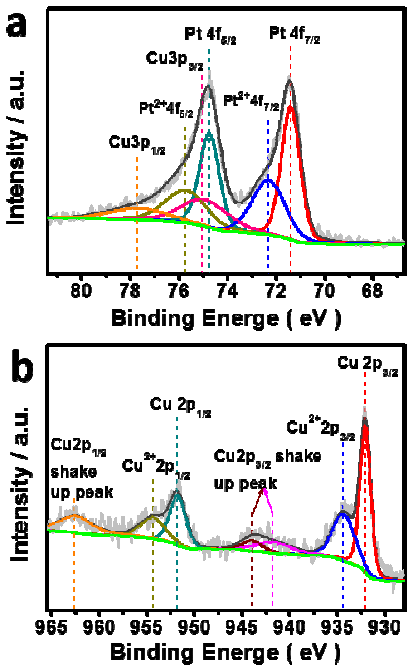

Fig. 4. (a) Pt4f XPS spectra and (b) Cu2p XPS spectra of PtCu/C nanoparticles

enclosed by (111) facets. This observation agrees well with the high-resolution TEM (HRTEM) image, which shows the d-spacing of 0.22 nm for (111) plane from three directions (Fig.1c).

The composition and valence state of the alloyed PtCu/C catalyst were further examined by X-ray photoelectron spectroscopy (XPS). Fig.S5a shows the wide survey spectrum of PtCu/C catalyst, revealing the presence of C, O, Cu and Pt elements. The Pt 4f spectra (Fig.4a) displays that Pt 4f region in the PtCu/C spectrum can be divided into two pairs of doublets. Two Pt 4f peaks were located at 71.5 and 74.8 eV, which can be assigned to the Pt 4f7/2 and Pt 4f5/2 of metallic Pt(0), respectively. The weaker doublet at 72.3 and 75.7 eV can be assigned to Pt in oxidized forms in the surface of sample. Besides, we noticed there are a third pair peak at the position of 74.9 eV and 77.66 eV. They were Cu3p peaks and Cu3p peaks would be bound to appear in the XPS spectra of this metal in theory if one metal was doped with Cu according to the knowledge of XPS. The Cu2p spectrum (Figure 3d) shows that, although most of the Cu is in the form of metallic Cu(0) (932.1eV and 957.77 eV), a weak signal from Cu(II) (934.34 eV and 954.32 eV) also exists. The presence of a small amount of Cu(II), further confirmed by a satellite peak at 943.9 eV and 941.63eV, can be attributed to the oxidation of surface Cu atoms in air. The existence of shake up peaks of Cu2p was also caused by Cu(II). Fig.S5b and Fig.S5c are C1s and O1s region in the PtCu/C spectrum, respectively, showing the carbon (C) element and oxygen (O) element existence of the sample. Based on the XPS results of PtCu/C catalyst, Pt and Cu are mainly in zero valence, and in alloy state on the surface of

PtCu/C catalyst. Pt is the most active mono metal for catalysis and it is well-known that alloying Pt with other transition metals can lower the electron binding energy of Pt and promote the C–H cleavage reaction at low potentials. In addition, alloying Pt with Cu, possible electronic or strain effects can improve the catalytic activity[34-37]. According to the XPS data, the average composition from the top surface region is about $Pt_{59}Cu_{41}$. The higher Pt content in the surface region than the overall PtCu based on the XRD result indicate the ligaments of the alloyed PtCu have a Pt-rich outmost surface. Although the XPS data cannot provide direct evidence on the formation of a core–shell structure, the composition variation indicates that the ligament surface contains a relatively high Pt amount.

The part of as-prepared PtCu nanoparticles were loaded on commercial carbon powder support and tested for their electrocatalytic activity for the MOR in a 0.5 M H_2SO_4 + 1 M CH_3OH aqueous solution at 30 ℃. The commercial catalyst (E-TEK Pt/C) was used to be a benchmark of the performance of the alloy catalysts. The electrochemical active surface areas (ECSAs) of PtCu NPs, carbon-supported PtCu nanoparticles and the commercial Pt/C catalyst were determined by cyclic voltammetry (Fig.5a), in which the current densities are normalized by the geometric area of the working electrode (0.196 cm^{-2}). The ECSAs, which were calculated by integrating the charge associated with the hydrogen adsorption/ desorption potential region after double-layer correction, are 7.042 $m^2\ g^{-1}$ for alloyed PtCu nanoparticles, 14.8$m^2\ g^{-1}$ for PtCu/C catalysts, and 26 $m^2\ g^{-1}$ for commercial Pt/C catalyst, respectively. The lower ECSAs of PtCu alloy nanoparticles are most likely due to the presence of residual impurities adsorbed on the surface and the larger sizes compared with Pt nanoparticles (ca. 3 nm) in commercial catalyst[18, 38].

For all the catalysts, the peak between 0.5 and 0.7 V in the forward scan is attributed to the electro-oxidation of methanol. The anodic peak at ~0.4 V in the backward scan is associated with the reactivation of oxidized Pt[39]. The voltammograms for MOR of PtCu nanoparticles, PtCu/C catalysts as well as commercial Pt/C catalyst were given in Fig.5b. Importantly, the peak current densities on the PtCu nanoparticles are 34.81 $mAcm^{-2}$, while the peak current densities on the PtCu/C catalysts are 24.6 mA cm^{-2}, which are all much higher than that on the Pt/C catalyst (5.6 mA cm^{-2}), as shown in Fig.5b. Noticeably, the peak current density of PtCu nanoparticles and PtCu/C catalysts are about 6.216 times and 4.4 times larger than that of Pt/C catalyst, respectively.

As shown in Fig.S6, the mass activity of PtCu/C is 1338.2mA mg^{-1}_{Pt}, which is higher than PtCu (1137.12 mA mg^{-1}_{Pt}) and Pt/C (480.3 mA mg^{-1}_{Pt}). Also, the mass activity of PtCu/C was compared with the synthesized $Pt_{68}Cu_{32}$ NPs (490.8 mA mg^{-1}_{Pt}), $Pt_{38}Cu_{62}$ NPs (393.7 mA mg^{-1}_{Pt}), individual component Pt nanoparticles (196.2 mA mg^{-1}_{Pt}) and Cu (0 mA mg^{-1}_{Pt}), as shown in Fig.S7. According to Table. S1, the mass activity of the as-made PtCu NPs is superior to that of previously reported stars-like PtCu/rGO (670 mA mg^{-1}_{Pt}), hollow-PtCu/C

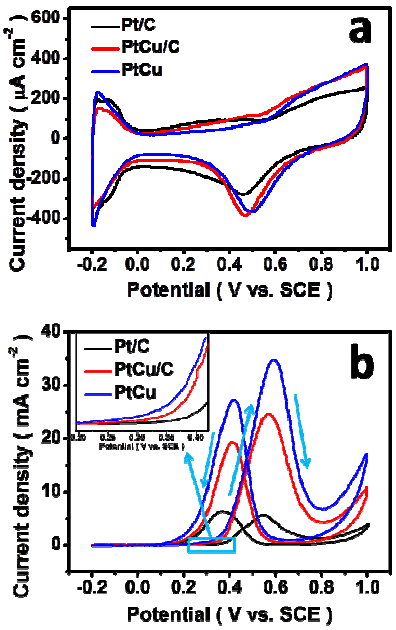

Fig. 5. (a) CVs of PtCu NPs (blue), PtCu/C (red) and Pt/C (black) at 50 mV/s in 0.5 M H_2SO_4, (b) CVs of MOR on PtCu NPs (blue), PtCu/C (red) and Pt/C (black) at 50 mV/s in 0.5M H_2SO_4 containing 1 M CH_3OH. Potential scan rate of 50 mV/s.

(889 mA mg^{-1}_{Pt}), nanoporous $Pt_{60}Cu_{40}$ (750 mA mg^{-1}_{Pt}), PtCu/C clusters (1200mA mg^{-1}_{Pt}), Pt_3Cu icosahedra (736 mA mg^{-1}_{Pt}) and $PtCu_2$/rGO (642 mA mg^{-1}_{Pt})[7, 12, 26, 40-42], and almost equals to Pt-C/C (1365 mA mg^{-1}_{Pt})[43]. These results further confirm the high catalytic activity of the PtCu nanoparticles. Moreover, we can also judge the catalytic activity from the half wave potential and the lower value shows a better activity of the catalyst. Table S2 shows that the half wave potential of PtCu, PtCu/C and Pt/C are 0.409 V, 0.426 V and 0.452 V, further confirming that the PtCu nanoparticles and PtCu/C catalyst possesses the higher catalytic activity.

To understand the difference of resistance to CO poison in catalytic activity of these two kinds of catalysts for MOR, the CO stripping tests for the PtCu nanoparticles, PtCu/C catalyst and commercial Pt/C catalyst were conducted. As shown in Fig.6, the onset potential of CO oxidation for the PtCu nanoparticles and PtCu/C catalyst appeared at 0.405 V, about 80 mV more negative than that on commercial Pt/C catalyst (0.485mV). These results demonstrate a very high activity of the PtCu/C NPs toward CO oxidation. The ease of CO removal over PtCu nanoparticles and PtCu/C catalyst relative to commercial Pt/C catalyst may reflect the effectiveness of electron coupling between the Cu and Pt in the alloyed nanoparticles. Moreover, that surface of the PtCu nanoparticles are enclosed with (111) plane can also explain this, as the adsorption of poisoning species is lowest on Pt(111)[21].

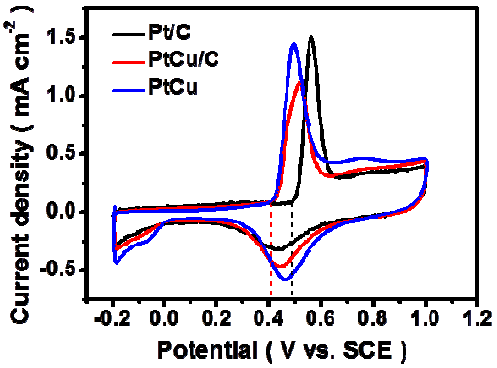

Fig. 6. CO stripping voltammograms of PtCu NPs (blue), PtCu/C (red) and Pt/C (black) with a saturated CO adlayer in CO-free 0.5 M H_2SO_4 . Potential scan rate of 50 mV/s.

To illustrate the stability of PtCu nanoparticles, continuous CV cycling from −0.2 to 1.0 V in 0.5 M H_2SO_4 + 1 M CH_3OH solution were tested. As shown in Fig.S8, the activities of all the catalysts decrease with increasing scan cycles. In Fig.S8(b) (d) and (f), after scanning 1000 cycles in 0.5 M H_2SO_4 + 1.0 M CH_3OH solution, the PtCu catalysts retain 79.33% of their initial values, and the PtCu/C catalysts keeps 75% of the origin value, whereas the commercial Pt/C catalyst drops to 64.6% of its initial value under the same testing conditions. Moreover, as shown in Fig.S8 (a) (c) and (e), the PtCu NPs showed high durability with a loss of 12.28% of the initial ECSAs, and the PtCu/C catalyst lost only 13.7% of the initial ECSAs after 1000 cycles of methanol oxidation. In sharp contrast, the commercial Pt/C catalyst lost 47.4% of their ECSAs after 1000 cycles of methanol oxidation reaction. Besides, Fig.S9 shows the shape and dispersion of PtCu NPs coated on carbon slightly changed after scanning 1000 cycles. While, the Pt particles in Pt/C contact with each other and would be more easily suffer from dissolution and Oswald ripening and form larger sized nanoparticles. As shown in Fig. S10, the shape and dispersion of Pt particles of Pt/C are seriously changed after 1000 cycles. These results show large decrease in ECSAs and activity. All these explain the better stability of PtCu nanoparticles. In summary, PtCu alloy NPs exhibit excellent activity and durability in electro-catalytic oxidation of methanol.

Conclusions

In conclusion, we have first demonstrated here a facile and general approach that could allow the one-pot fabrication of uniform monodispersed and self-assembled multi-crystalline PtCu alloyed nanospheres. Alloyed PtCu nanospheres were successfully prepared by the simultaneous reduction of H_2PtCl_6 and $Cu(NO_3)_2{\cdot}3H_2O$ in the presence of DMF and CTAB. The nanoparticles were characterised by TEM, PXRD and XPS to determine their physical properties. The electrochemical catalytic activity of these PtCu nanospheres towards methanol oxidation was also evaluated in comparison with the activity of commercial Pt/C. The PtCu NPs and PtCu/C catalysts had a superior electrocatalytic activity than the commercial Pt/C catalysts.

Acknowledgements

This work was supported by the Major International (Regional) Joint Research Project (51210002) and the National Basic Research Program of China (2015CB932304). PKS acknowledge the support from the Danish project of Initiative toward Non-precious Metal Polymer Fuel Cells (4106-000012B).

Notes and references

1. M. L. Foo, Y. Wang, S. Watauchi, H. Zandbergen, T. He, R. Cava and N. Ong, *Physical Review Letters*, 2004, **92**, 247001.
2. Y. Cheng, C. Xu, P. K. Shen and S. P. Jiang, *Applied Catalysis B: Environmental*, 2014, **158**, 140-149.
3. U. Paulus, T. Schmidt, H. Gasteiger and R. Behm, *Journal of Electroanalytical Chemistry*, 2001, **495**, 134-145.
4. B. C. Steele and A. Heinzel, *Nature*, 2001, **414**, 345-352.
5. Z. Liu, X. Y. Ling, X. Su and J. Y. Lee, *The Journal of Physical Chemistry B*, 2004, **108**, 8234-8240.
6. D.-M. Gu, Y.-Y. Chu, Z.-B. Wang, Z.-Z. Jiang, G.-P. Yin and Y. Liu, *Applied Catalysis B: Environmental*, 2011, **102**, 9-18.
7. D. Chen, Y. Zhao, X. Peng, X. Wang, W. Hu, C. Jing, S. Tian and J. Tian, *Electrochimica Acta*, 2015,**177**,86-92.
8. E. Antolini, *Applied Catalysis B: Environmental*, 2007, **74**, 337-350.
9. K. Friedrich, K. Geyzers, A. Dickinson and U. Stimming, *Journal of Electroanalytical Chemistry*, 2002, **524**, 261-272.
10. Y. Yamauchi, A. Tonegawa, M. Komatsu, H. Wang, L. Wang, Y. Nemoto, N. Suzuki and K. Kuroda, *Journal of the American Chemical Society*, 2012, **134**, 5100-5109.
11. Y. Yu, W. Yang, X. Sun, W. Zhu, X.-Z. Li, D. Sellmyer and S. Sun, *Nano Letters*, 2014, **14**, 2778-2782.
12. X. Peng, Y. Zhao, D. Chen, Y. Fan, X. Wang, W. Wang and J. Tian, *Electrochimica Acta*, 2014, **136**, 292-300.
13. Z. L. Zhao, L. Y. Zhang, S. J. Bao and C. M. Li, *Applied Catalysis B: Environmental*, 2015, **174**, 361-366.
14. X. Lei, M. Wu, G. Liu, B. Xu and C. Ouyang, *The Journal of Physical Chemistry A*, 2013, **117**, 8293-8297.
15. G. Cui, P. K. Shen, H. Meng, J. Zhao and G. Wu, *Journal of Power Sources*, 2011, **196**, 6125-6130.
16. Y. Liu, Y. Huang, Y. Xie, Z. Yang, H. Huang and Q. Zhou, *Chemical Engineering Journal*, 2012, **197**, 80-87.
17. R. Amin, R. A. Hameed, K. El-Khatib, H. El-Abd and E. R. Souaya, *International Journal of Hydrogen Energy*, 2012, **37**, 18870-18881.
18. L. Han, P. Cui, H. He, H. Liu, Z. Peng and J. Yang, *Journal of Power Sources*, 2015, **286**, 488-494.
19. I. Mintsouli, J. Georgieva, S. Armyanov, E. Valova, G. Avdeev, A. Hubin, O. Steenhaut, J. Dille, D. Tsiplakides and S. Balomenou, *Applied Catalysis B: Environmental*, 2013, **136**, 160-167.
20. Y. Kang, J. B. Pyo, X. Ye, R. E. Diaz, T. R. Gordon, E. A. Stach and C. B. Murray, *ACS Nano*, 2012, **7**, 645-653.
21. Y. Kang, M. Li, Y. Cai, M. Cargnello, R. E. Diaz, T. R. Gordon, N. L. Wieder, R. R. Adzic, R. J. Gorte and E. A.

Stach, *Journal of the American Chemical Society*, 2013, **135**, 2741-2747.
22. X. Huang, S. Tang, X. Mu, Y. Dai, G. Chen, Z. Zhou, F. Ruan, Z. Yang and N. Zheng, *Nature Nanotechnology*, 2011, **6**, 28-32.
23. Y. Kang, X. Ye and C. B. Murray, *Angewandte Chemie International Edition*, 2010, **49**, 6156-6159.
24. W. Zhou, J. Wu and H. Yang, *Nano Letters*, 2013, **13**, 2870-2874.
25. J. Wu, L. Qi, H. You, A. Gross, J. Li and H. Yang, *Journal of the American Chemical Society*, 2012, **134**, 11880-11883.
26. X. Huang, Y. Chen, E. Zhu, Y. Xu, X. Duan and Y. Huang, *Journal of Materials Chemistry A*, 2013, **1**, 14449-14454.
27. H. Yang, J. Zhang, S. Kumar, H. Zhang, R. Yang, J. Fang and S. Zou, *Electrochemistry Communications*, 2009, **11**, 2278-2281.
28. S. Mourdikoudis and L. M. Liz-Marzán, *Chemistry of Materials*, 2013, **25**, 1465-1476.
29. B. Lee, P. Podsiadlo, S. Rupich, D. V. Talapin, T. Rajh and E. V. Shevchenko, *Journal of the American Chemical Society*, 2009, **131**, 16386-16388.
30. J. Henzie, M. Grünwald, A. Widmer-Cooper, P. L. Geissler and P. Yang, *Nature Materials*, 2012, **11**, 131-137.
31. N. Goubet, J. Richardi, P. A. Albouy and M. P. Pileni, *Advanced Functional Materials*, 2011, **21**, 2693-2704.
32. C. Murray, C. Kagan and M. Bawendi, *Science*, 1995, **270**, 1335-1338.
33. M. Pileni, *Accounts of Chemical Research*, 2012, **45**, 1965-1972.
34. V. R. Stamenkovic, B. Fowler, B. S. Mun, G. Wang, P. N. Ross, C. A. Lucas and N. M. Marković, *Science*, 2007, **315**, 493-497.
35. I. E. Stephens, A. S. Bondarenko, F. J. Perez-Alonso, F. Calle-Vallejo, L. Bech, T. P. Johansson, A. K. Jepsen, R. Frydendal, B. P. Knudsen and J. Rossmeisl, *Journal of the American Chemical Society*, 2011, **133**, 5485-5491.
36. M. Oezaslan, M. Heggen and P. Strasser, *Journal of the American Chemical Society*, 2011, **134**, 514-524.
37. I. Dutta, M. K. Carpenter, M. P. Balogh, J. M. Ziegelbauer, T. E. Moylan, M. H. Atwan and N. P. Irish, *The Journal of Physical Chemistry C*, 2010, **114**, 16309-16320.
38. P. Mani, R. Srivastava and P. Strasser, *The Journal of Physical Chemistry C*, 2008, **112**, 2770-2778.
39. E. Antolini, J. R. Salgado and E. R. Gonzalez, *Applied Catalysis B: Environmental*, 2006, **63**, 137-149.
40. H.-J. Qiu, X. Shen, J. Wang, A. Hirata, T. Fujita, Y. Wang and M. Chen, *ACS Catalysis*, 2015,**5**,3779-3785.
41. Q. Lv, J. Chang, W. Xing and C. Liu, *RSC Advances*, 2014, **4**, 32997-33000.
42. X. Sun, K. Jiang, N. Zhang, S. Guo and X. Huang, *ACS Nano*, 2015, ***9***, 7634–7640.
43. M. Huang and L. Guan, *International Journal of Hydrogen Energy*, 2015, **40**, 6546-6551.

TOC

*Xuewei Du, Shuiping Luo, Hongyu Du, Min Tang, Xiangdong Huang, and Pei Kang Shen**

Page No. – Page No.

Monodisperse and self-assembled Pt-Cu nanoparticles as an efficient electrocatalyst for methanol oxidation reaction

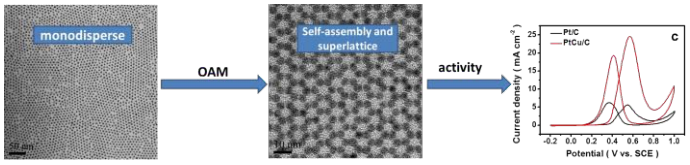

The monodispersed PtCu nanoparticles have been synthesized and can be self-assembled into superlattice and it shows 4.4 times in activity, higher stability compared with Pt/C and better CO tolerance toward methanol oxidation reaction.